BRAIN COMMUNICATIONS

AAV1.NT-3 gene therapy in a CMT2D model: phenotypic improvements in *Gars^P278KY/+* mice

Burcak Ozes,[1] Kyle Moss,[1] Morgan Myers,[1] Alicia Ridgley,[1] Lei Chen,[1] Darren Murrey[1] and
🆔Zarife Sahenk[1,2,3]

Glycyl–tRNA synthetase mutations are associated to the Charcot–Marie–Tooth disease type-2D. The *Gars^P278KY/+* model for Charcot–Marie–Tooth disease type-2D is known best for its early onset severe neuropathic phenotype with findings including reduced axon size, slow conduction velocities and abnormal neuromuscular junction. Muscle involvement remains largely unexamined. We tested the efficacy of neurotrophin 3 gene transfer therapy in two Gars mutants with severe (*Gars^P278KY/+*) and milder (*Gars^ΔETAQ/+*) phenotypes via intramuscular injection of adeno-associated virus setoype-1, triple tandem muscle creatine kinase promoter, neurotrophin 3 (AAV1.tMCK.NT-3) at 1×10^{11} vg dose. In the *Gars^P278KY/+* mice, the treatment efficacy was assessed at 12 weeks post-injection using rotarod test, electrophysiology and detailed quantitative histopathological studies of the peripheral nervous system including neuromuscular junction and muscle. Neurotrophin 3 gene transfer therapy in *Gars^P278KY/+* mice resulted in significant functional and electrophysiological improvements, supported with increases in myelin thickness and improvements in the denervated status of neuromuscular junctions as well as increases in muscle fibre size along with attenuation of myopathic changes. Improvements in the milder phenotype *Gars^ΔETAQ/+* was less pronounced. Furthermore, oxidative enzyme histochemistry in muscles from Gars mutants revealed alterations in the content and distribution of oxidative enzymes with increased expression levels of *Pgc1a*. C*ox1, Cox3* and *Atp5d* transcripts were significantly decreased suggesting that the muscle phenotype might be related to mitochondrial dysfunction. Neurotrophin 3 gene therapy attenuated these abnormalities in the muscle. This study shows that neurotrophin 3 gene transfer therapy has disease modifying effect in a mouse model for Charcot–Marie–Tooth disease type-2D, leading to meaningful improvements in peripheral nerve myelination and neuromuscular junction integrity as well as in a unique myopathic process, associated with mitochondria dysfunction, all in combination contributing to functional outcome. Based on the multiple biological effects of this versatile molecule, we predict neurotrophin 3 has the potential to be beneficial in other aminoacyl-tRNA synthetase-linked Charcot–Marie–Tooth disease subtypes.

1　Department of Pediatrics, Center for Gene Therapy, The Abigail Wexner Research Institute, Nationwide Children's Hospital, Columbus, OH 43205, USA
2　Department of Pediatrics and Neurology, Nationwide Children's Hospital and The Ohio State University, Columbus, OH 43205, USA
3　Department of Pathology and Laboratory Medicine, Nationwide Children's Hospital, Columbus, OH 43205, USA

Correspondence to: Zarife Sahenk, MD, PhD
Director, Neuromuscular Pathology
700 Children's Drive Rm WA 3024
Columbus, OH 43205, USA
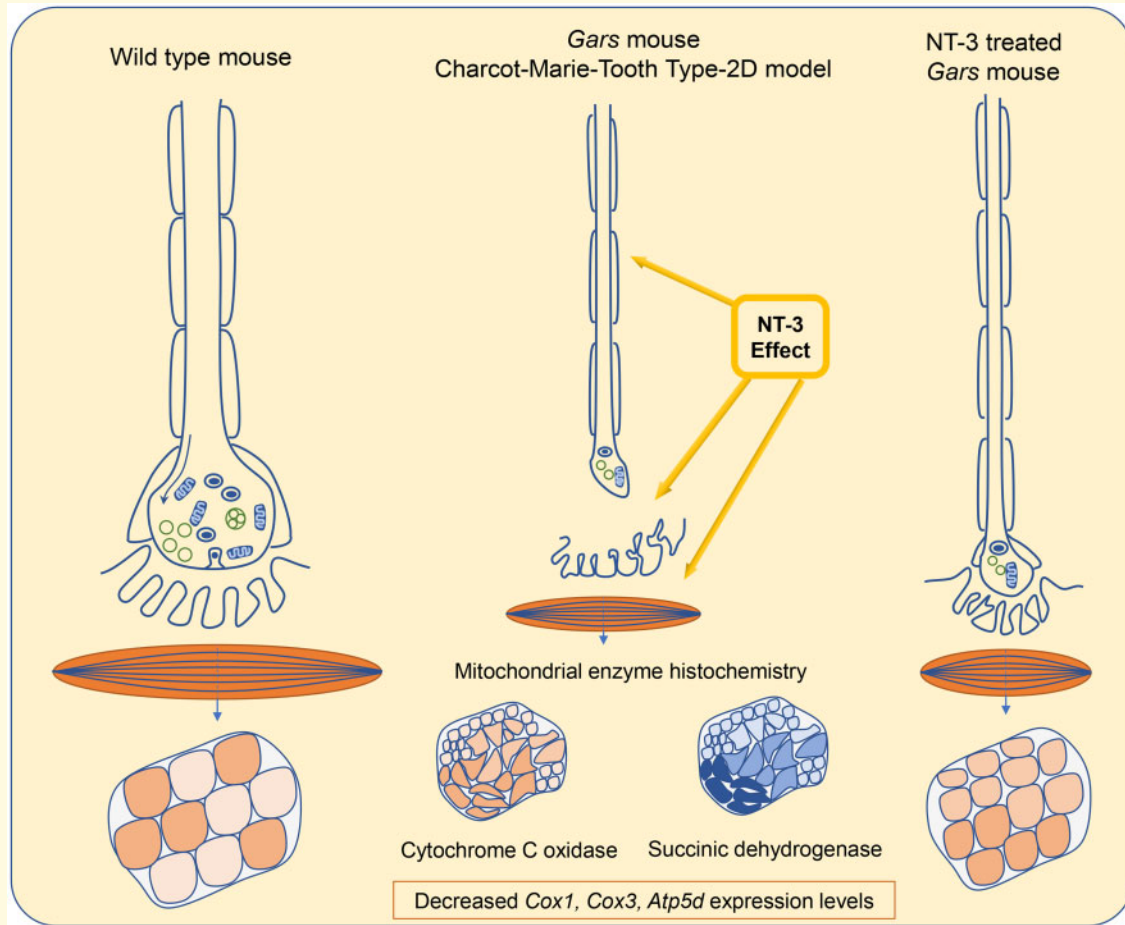E-mail: zarife.sahenk@nationwidechildrens.org

---

Graphical Abstract

Introduction

Mutations in several aminoacyl–tRNA synthetase (ARS) genes have been linked to different forms of Charcot–Marie–Tooth disease.[1–6] ARSs are ubiquitously expressed enzymes responsible for charging tRNAs with their cognate amino acids, the essential first step in protein synthesis. The nuclear-encoded glycyl–tRNA synthetase gene (*GARS1*) is required for protein translation in both cytoplasm and mitochondria.[7] So far, autosomal-dominant missense/nonsense, splicing and small deletions in *GARS1* are known to present with axonal type Charcot–Marie–Tooth disease type-2D, distal hereditary motor neuronopathy type VA[1] or infantile spinal muscular atrophy, James type (resulting from *de novo* heterozygous missense mutations),[8,9] while some autosomal recessive mutations have been reported to display a wide range of conditions compatible with mitochondrial phenotype including early-onset severe cardiomyopathy, exercise-induced myalgia, increased lactate, periventricular white matter brain lesions or multi-system disease with growth retardation.[10–13] Extensive studies of compound heterozygous *GARS1* variants from patients with mitochondria phenotype lead to a conclusion that these mutations are associated with loss of function. Contrary, studies in the rodent model for Charcot–Marie–Tooth disease type-2D showing dominant mutations in *Gars* were thought secondary to a toxic gain of function with a neuropathic phenotype that could not be corrected by overexpression of wildtype (WT) *Gars*.[14–16] The downstream events explaining tissue-specific phenotype–genotype relations, however, remain unclear. Studies using human-induced neuronal progenitor cells (iNPCs) carrying dominant and recessive GARS mutations have emphasized underlying mitochondrial dysfunction with alterations of mitochondrial proteins, which were found more prominent in iNPCs with dominant neuropathy-causing mutations.[17] However, mitochondrial functions have gone largely unexamined in the disease and its models.

Neurotrophin 3 (NT-3) is an important autocrine factor supporting Schwann cell survival and differentiation and stimulates axon regeneration and myelination.[18–20] Other biological effects of NT-3 relevant to this study include its role in the maintenance of neuromuscular junction (NMJ) integrity, radial growth of muscle fibres through activation

of Akt/mTOR pathway and the activation of mitochondria biogenesis regulator, peroxisome proliferator-activated receptor γ coactivator 1 alpha (PGC1α) in neurogenic muscle.[21]

NT-3 gene therapy via intramuscular injection provides sustained NT-3 delivery through secretion by the muscle cells.[20] In this study, we tested the efficacy of NT-3 gene transfer therapy using self-complementary adeno-associated virus serotype 1 (scAAV1) and triple muscle-specific creatine kinase (tMCK) promoter[22,23] in two Charcot–Marie–Tooth disease type-2D mouse models with different *GARS* mutations: the strain with a severe phenotype, CAST; B6-Gars[Nmf249]/Rwb, which was extensively used in previous studies and also referred as $Gars^{P278KY/+}$, and B6; FVB-Gars<em2Rwb>/Rwb, referred as $Gars^{\Delta ETAQ/+}$ with a milder phenotype.[24] The treatment efficacy was assessed using rotarod test, electrophysiology and detailed quantitative histopathological studies of the peripheral nervous system including NMJ and muscle.

Collectively, these studies have shown that AAV1.NT-3 gene therapy in $Gars^{P278KY/+}$ mice resulted in significant functional and electrophysiological improvements, supported with increases in myelin thickness and improvements in the denervated status of NMJs as well as increases in muscle fibre size along with attenuation of myopathic changes. Improvements in the milder phenotype $Gars^{\Delta ETAQ/+}$ was less pronounced. In addition, we found no evidence of length-dependent axonal loss at distal tibial nerves (dying-back process typical for classical Charcot–Marie–Tooth phenotype),[25] therefore, furthering the classification of the neuropathic process as distal-terminal axonopathy. Additional characterization of these *Gars* mutants using routine histopathology and oxidative enzyme histochemistry in muscle revealed the presence of a primary myopathic process associated with alterations in the content and distribution of oxidative enzymes in muscle and increased expression levels of *Pgc1a*, which is an important transcriptional coactivator of mitochondrial biogenesis and respiration.[26] Moreover, complex I, III and *Atp5d* transcripts were significantly decreased suggesting that the muscle phenotype might be related to mitochondrial dysfunction. NT-3 gene therapy attenuated these abnormalities in muscle, which we report here as a novel finding.

Materials and methods

Animals and treatment groups

Two different Charcot–Marie–Tooth disease type-2D mouse models obtained from the Jackson Laboratory were included in the study. The initial characterization of $Gars^{P278KY/+}$ (B6; CAST-Gars[Nmf249]/RwbJ, JAX stock #033165) and $Gars^{\Delta ETAQ/+}$ mice have been described previously.[24,27] Heterozygous $Gars^{P278KY/+}$ and $Gars^{\Delta ETAQ/+}$ mice were outbred with C57BL/6 mice and heterozygous offspring were used. Genotypes were established by PCR analysis of genomic DNA isolated from tail clips. All animal experiments were performed according to the ethical guidelines approved by The Research Institute at Nationwide Children's Hospital Animal Care and Use Committee (IACUC approval number: AR18-00076).

Four to six weeks old $Gars^{P278KY/+}$ mice (6 females and 7 males, $n = 13$) and of 8–10 weeks old $Gars^{\Delta ETAQ/+}$ (6 females and 5 males, $n = 11$) were injected with 1×10^{11} vg (qPCR titer with supercoiled standard) of scAAV1.tMCK.NT-3 vector equally divided into right and left gastrocnemius muscles. Age-matched $Gars^{P278KY/+}$ (4 females and 4 males, $n = 8$) and $Gars^{\Delta ETAQ/+}$ (5 females and 7 males, $n = 12$) mice injected with Ringer's lactate served as controls. Over-dosage of xylazine/ketamine anaesthesia was used to euthanize $Gars^{P278KY/+}$ mice at 12 weeks, and $Gars^{\Delta ETAQ/+}$ mice at 30 weeks post-gene treatment.

rAAV.NT-3 vector production and potency

scAAV1 carrying the human NT-3 transgene under the control of tMCK promoter was previously described.[20] Vector was produced in the Viral Vector Core at Nationwide Children's Hospital, Columbus, USA. Blood samples were collected by cardiac puncture after anaesthetizing the treated and untreated mice at the corresponding endpoints. Serum NT-3 levels were assessed by ELISA test as previously reported.[20]

Rotarod testing

Accelerating rotarod (Columbus Instruments, Ohio, USA) was used to test mouse motor function and balance. $Gars^{P278KY/+}$ mice were tested at baseline and endpoint and the performance of $Gars^{\Delta ETAQ/+}$ mice was examined at the endpoint. Mice were acclimated to the rotarod apparatus at least 24 h prior to the test run. The protocol was run at 5 rpm with a constant acceleration of 0.2 rpm/s for $Gars^{P278KY/+}$ mice and 0.5 rpm/s for $Gars^{\Delta ETAQ/+}$ mice. The average of the best two out of three runs was included in the analysis.

Nerve conduction studies

The animals were anaesthetized under 2% isoflurane and a heating pad was used to maintain body temperature at 37°C. Nerve conduction studies were performed on the right sciatic using a Nicolet Viasys Viking Select EMG EP System (Nicolet Biomedical, Wisconsin, USA); 27 G disposable needle electrodes were used for both stimulation and recording as described previously.[28]

Peripheral nerve histology and quantitative studies

The sciatic and tibial nerves were removed under a dissecting microscope. Tissues were fixed in glutaraldehyde

and were embedded in plastic for light microscopy using previously described standard methods.[29] Samples were selected for morphometric analysis based on the suitability of the tissue sections, including staining quality, contrast and lack of artefacts such as wrinkles in the section, and not based on outcomes of behavioural or physiological analyses.

Myelinated fibre density determinations

One μm-thick toluidine blue-stained cross-sections from mid sciatic and tibial nerve segments from treated and untreated cohorts and age-matched WT mice were analysed. Five randomly selected areas (one from the centre and four from each quadrant) were photographed at ×100 magnification and axon diameter measurements were obtained from the computer screen image frames using BioQuant Life Sciences imaging software as previously described (2014, V15.5.6; BioQuant Image Analysis Corporation, Nashville, Tennessee).[28] A total of 0.0502 mm^2 of endoneurial area per mouse was analysed. Composites of fibre size distribution histograms expressed as number per 0.01 mm^2 of endoneurial areas and mean myelinated fibre (MF) densities (mean ± SEM, number/ 0.1 mm^2) were generated. Measurements from age-matched WT mice were also generated for comparison.

G ratio of the MFs

Measurements were done by outlining the myelin interior and exteriors in AxioVision (AxioVs40x64 V 4.9.1.0) to determine the area, which was used to derive diameters to yield g-ratio, as described previously.[28] For each animal, measurements from all MFs in three random images (photographed at ×100 magnification) from mid-sciatic nerves were obtained from scAAV1.tMCK.NT-3 injected and untreated $Gars^{P278KY/+}$ and $Gars^{\Delta ETAQ/+}$ mice to generate scattergrams and the percent g ratio distribution histograms. Slopes of AAV.NT3 treated versus untreated were compared using GraphPad software (GraphPad Prism 8.2.0).

Histological analysis of muscle

Gastrocnemius and tibialis anterior muscles from scAAV1.tMCK.NT-3 and Ringer's lactate injected $Gars^{P278KY/+}$ mice and $Gars^{\Delta ETAQ/+}$ mice with an equal number of males and females in each group were cut to 12 μm thick cross cryostat sections and were stained with H&E. Details of quantitative analysis of muscle is given in the Supplementary data. Histochemical assessment of mitochondria function was done in gastrocnemius muscles from $Gars^{P278KY/+}$ mice and $Gars^{\Delta ETAQ/+}$ mice using cytochrome c oxidase (COX) and succinic dehydrogenase (SDH) enzyme histochemistry protocols established in our laboratory.

Immunohistochemical analysis of NMJs

Lumbrical muscles[30] from $Gars^{P278KY/+}$ and $Gars^{\Delta ETAQ/+}$ mice were processed (antibodies: acetylcholine receptor antibody, α-bungarotoxin, T1175, 1:500; anti-neurofilament 200 antibody, N4142, 1:500; SV2 antibody, AB_2315387, 1:50)[31,32] and interpreted[27] as described previously (details in the Supplementary data).

RNA isolation and mRNA expression

Total RNA was isolated from muscles tissues using the QIAzol lysis reagent, treated with DNase and purified using RNeasy Plus Universal Kit (Qiagen). ProtoScript II cDNA Synthesis Kit (New England Biolabs) was used for first-strand DNA synthesis. Primer sets for *PGC-1α*, *Cox1*, *Cox3* and *Atp5d* were obtained from previous publications[33–35] (details in the Supplementary data).

Quantification of mitochondrial DNA

Total DNA was isolated using the QIAamp DNA Mini Kit (Qiagen). Primers for mitochondrial (mtDNA) and genomic DNA were obtained from previous publication.[36] qPCR was performed using SYBR Green Master Mix and the 7500 Fast Real-Time PCR detection system (Applied Biosystems). Quantification was performed as given in the previous publication[37] by normalizing quantity of mtDNA to genomic DNA.

Primary myoblast cell culture

Skeletal muscles were collected from two 4 weeks old $Gars^{P278KY/+}$ mice and two age-matched C57BL/6 mice. Protocol was adapted from previous publications[38,39] (details in the Supplementary data). Randomly selected areas were photographed at ×20 magnification (Nikon Eclipse Ti2-E, Japan). Fusion index was calculated for each image as a percentage of the total number of nuclei in myotubes (more than one nucleus) out of the total number of nuclei.

Statistical analysis

Adequate sample size was determined according to our previous studies that performed analogous experiments.[28,40] For comparisons between treated and non-treated groups, statistical analyses were performed in GraphPad Prism 8.2 software. Two-tail Student's *t*-test, one-way ANOVA with Tukey's multiple comparison test, two-way ANOVA with Tukey's or Bonferonni's multiple comparison test or linear regression analysis were performed based on the data, and the significance level was set at $P \leq 0.05$. The tests that meet the best assumptions

of the data were chosen. Results were given as mean ± SEM in all experiments and the number of animals was mentioned in figure legends along with the name of the statistical analysis performed. Other than the functional tests, no blinding was used. Blinding was not possible for histopathological analysis due to the presence of recognizable treatment effects.

Data availability

The data that support the findings of the study are available from the corresponding author upon reasonable request.

Results

rAAV.NT-3 vector production and potency

scAAV1.tMCK.NT-3 design (Supplementary Fig. 1A) and production followed previously described methods at Nationwide Children's Hospital, Columbus.[20] scAAV1.tMCK.NT-3 was delivered to the gastrocnemius muscle of two mouse models of Charcot–Marie–Tooth disease type-2D, $Gars^{P278KY/+}$ representing a severe phenotype and $Gars^{\Delta ETAQ/+}$, a milder phenotype; blood samples from anaesthetized treated and untreated mice were collected by cardiac puncture at 12- and 30-weeks post-gene delivery, respectively. Serum NT-3 levels were detected in the treated cohorts (Supplementary Fig. 1B) using a capture ELISA as previously reported.[20]

NT-3 gene transfer improves clinical phenotype of $Gars^{P278KY/+}$ mice

Functional and electrophysiological studies
Rotarod test was performed in $Gars^{P278KY/+}$ mice at 4 weeks post-gene injection as an initial evaluation (referred to as baseline) and at the endpoint when mice reached 17–18 weeks of age, 12 weeks after NT-3 gene transfer. The endpoint performance with treatment was significantly higher corresponding to a 33% increase compared to the untreated cohort (Fig. 1A). Compared to the initial evaluation (56.31 ± 5.54 s), the endpoint performance of the AAV1.NT-3 group increased 27% ($P = 0.044$), while the untreated group remained unchanged ($P = 0.90$). Improvements in the rotarod test in the treated group were associated with clinical observations of improved toe spreading (Supplementary Fig. 2A–D).

Sciatic nerve conduction outcome studies supported the efficacy of NT-3 gene transfer therapy. The nerve conduction velocities (NCV) were significantly improved with treatment resulting in a 42% increase in the sciatic NCV compared to the untreated cohort (Fig. 1B), which were slower than WT as reported previously.[27] Mean CMAP amplitude was also increased significantly in the

AAV1.NT-3-treated $Gars^{P278KY/+}$ mice (Fig. 1C and D), correlating with functional outcome.

We assessed the efficacy of scAAV1.tMCK.NT-3 delivery in the $Gars^{\Delta ETAQ/+}$ mutant when mice reached 10 (38–40 weeks) months of age, at 30 weeks post-gene delivery. Rotarod performance, CMAP and sciatic NCV values in the treated cohort were not statistically different from the untreated, which might be related to the milder manifestation of the phenotype in $Gars^{\Delta ETAQ/+}$ mice (Supplementary Fig. 3).

Efficacy of NT-3 gene transfer therapy in peripheral nerves of $Gars^{P278KY/+}$ and $Gars^{\Delta ETAQ/+}$ mice

Neuropathic process in Gars mutants is a distal-terminal axonopathy
$Gars$ mutants have early onset, severe sensory motor phenotype with reduced axon size and loss of NMJ connectivity.[24,27] It is not clear if there is an associated length-dependent distal axon loss. Compared to WT (Supplementary Fig. 4), peripheral nerves from $Gars^{P278KY/+}$ mice showed strikingly small axon size along with an increase in the density of MFs as illustrated in samples from ventral roots, mid sciatic and distal tibial nerves (Supplementary Fig. 4). To assess the efficacy of NT-3 gene therapy, it was important to have a detailed understanding of the disease process according to the anatomical site of involvement in peripheral nerves of the $Gars^{P278KY/+}$ model. One possibility is that the neuropathic process may be a length-dependent distal axonopathy causing axonal loss in distal nerves ('dying back' process[41]), a feature of many neuropathic conditions including classical Charcot–Marie–Tooth phenotype. To investigate this, we carried out detailed quantification of MFs (MF density per unit area of endoneurium, MF-axon size distribution and actual MF number per nerve) at mid-sciatic (proximal) and tibial nerves (distal) from $Gars$ mutants and age-matched WT controls (Supplementary Table 1).

In WT nerves, compared to sciatic nerve (proximal), the endoneurial cross-sectional area-decrease at the tibial level was about 70% and the mean density of MFs was 1.5 times higher than that of the proximal level. This density increase can be explained by the fact that in WT, axon size decreases along the nerve from proximal-distal direction.[42] In $Gars^{P278KY/+}$ nerves, we found significantly smaller endoneurial cross-sectional areas; there was also an increase in MF density about 2.6-fold at the sciatic level and 2-fold at the tibial level compared to WT nerves (Supplementary Table 1). Interestingly, however, the decrease in endoneurial cross-sectional area at tibial level (about 54%) was not as prominent as in WT, and proximal to distal MF density change was not significant, 1.15 times higher than that of the proximal level (Supplementary Fig. 4, depicting morphometric values
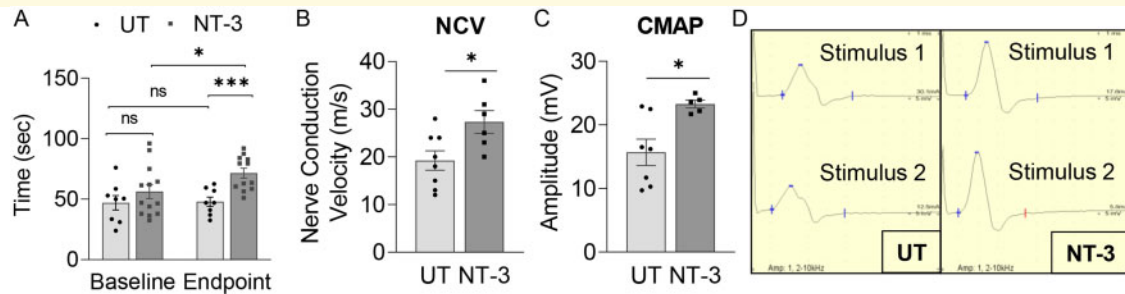
Figure 1 Efficacy of AAV1.NT-3 gene transfer therapy in *Gars*^P278KY/+ mice by functional and electrophysiological studies.
Rotarod performance of *Gars*^P278KY/+ mice, shown in **A**, tested at 12 weeks post-treatment showed significant improvement in the AAV1.NT-3-treated mice (NT-3: 71.54 s, $n = 12$ versus UT: 47.94 s, $n = 8$; $P = 0.0008$). There was no statistical difference between UT and NT-3-treated cohorts at baseline (47.06 s versus 56.31 s, $P = 0.30$). Over a 12-week time period, the performance of the treated mice improved (56.31 s versus 71.54 s, $P = 0.044$), while in the UT mice, no change was observed (47.06 s versus 47.94 s, $P = 0.90$). Sciatic nerve conduction studies in *Gars*^P278KY/+ mice performed at the endpoint is shown in **B**. NCV was significantly improved with treatment corresponding to a 42% increase compared to UT cohort ($P = 0.024$). CMAP was also increased in the NT-3 cohort compared to UT ($P = 0.013$), shown in **C**. Representative waveforms of the sciatic nerve motor nerve conduction from UT and NT-3 cohorts are shown in **D**; base time is 1 ms for both panels. Data are represented as mean ± SEM, unpaired *t*-test.
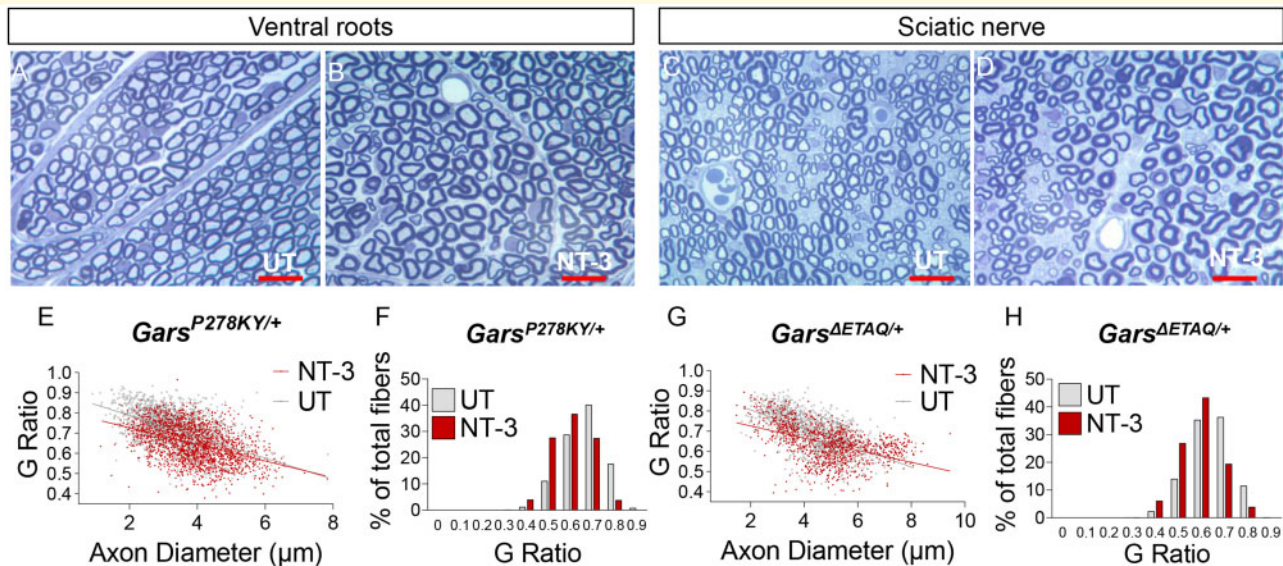

Figure 2 NT-3 gene transfer improves myelin thickness of peripheral nerves in *Gars*^P278KY/+ and *Gars*^ΔETAQ/+ mice.
Representative 1 μm-thick, toluidine blue-stained cross-sections of, shown in **A** and **B**, ventral roots and, shown in **C** and **D**, sciatic nerves from, shown in **A** and **C**, untreated and, shown in **B** and **D**, treated *Gars*^P278KY/+ mice. Scale bar = 10 μm. A notable increase of myelin thickness is seen with treatment, shown in **B** and **D**, compared to samples from untreated, shown in **A** and **B**. G ratios calculated for the sciatic nerve of the treated and untreated, shown in **E**, *Gars*^P278KY/+ and shown in **G**, *Gars*^ΔETAQ/+ mice are shown as scatterplots against respective axon diameters [total number of analysed MFs = 1840 for untreated (460 ± 45.1 measurements per mouse) and 1792 for NT-3 treated (448 ± 20.09 measurements per mouse) *Gars*^P278KY/+ mice and 1270 for untreated (317.5 ± 11.1 measurements per mouse) and 1042 for NT-3 treated (260.5 ± 20.1 measurements per mouse) *Gars*^ΔETAQ/+ mice; $n = 4$ per cohort]. Lines indicate linear regression. The slopes are significantly different between the two groups for both mutants (in **E**: NT-3, $r^2 = 0.1893$; UT, $r^2 = 0.2770$; Linear regression, $P < 0.0001$ and **G**: NT-3, $r^2 = 0.3545$; UT, $r^2 = 0.2279$; Linear regression, $P < 0.0001$). G-ratios shown as percent distribution indicate a shift to the left with an increase in the number of axons with thicker myelin with NT-3 gene transfer therapy in both *Gars*^P278KY/+, shown in **F**, and *Gars*^ΔETAQ/+ mice, shown in **H.**

from Supplementary Table 1). The analysis of proximo-distal MF-axon size distribution in WT sciatic nerves show a wide range of axon size distribution with diameters >6 μm, constituting 48% of all fibres; in the tibial nerve, this subpopulation was only 7%, confirming previous observations of decrease in proximodistal axon size[42] (Supplementary Fig. 5). In *Gars*^P278KY/+ nerves, however, due to a much narrower distribution of axon size and
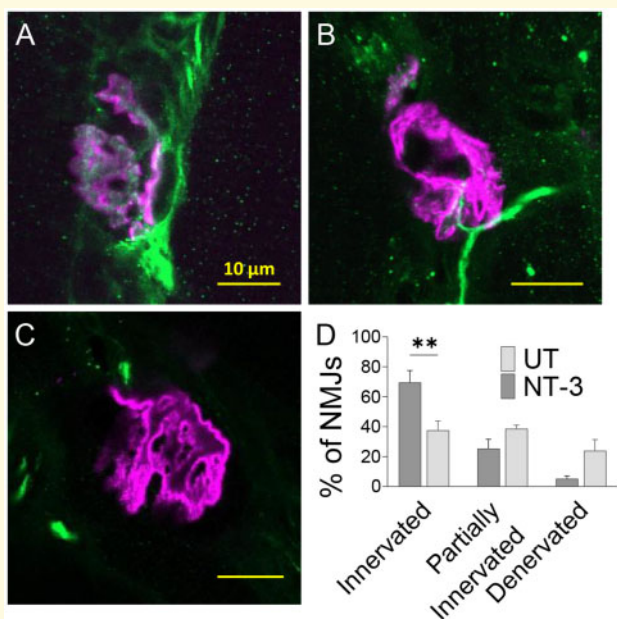
Figure 3 NT-3 gene transfer improves neuromuscular junction assembly in $Gars^{P278KY/+}$ mice. Representative images showing innervated, shown in **A**, partially innervated, shown in **B**, and denervated, shown in **C**, NMJs from the lumbrical muscles of the $Gars^{P278KY/+}$ mice, stained with IHC techniques. Scale bar = 10 μm. **D** shows innervated NMJs increased 32% in the treated mice (P = 0.0016). An average of 88.6 NMJs per mouse were evaluated from NT-3-treated and UT-mice (n = 6 mice per group). Data are represented as mean ± SEM; two-way ANOVA, Bonferroni's multiple comparisons test.

the absence of large-diameter axons, the proximodistal axon size change and resulting MF density increase appeared less pronounced. Moreover, the total number of MFs in the tibial nerve from $Gars^{P278KY/+}$ was not statistically different than that was obtained from the WT tibial nerve (Supplementary Table 1). In accordance with these qualitative data as well as our microscopic observations on the tibial nerve and intramuscular nerve bundles of lumbrical muscles, which showed no evidence of acute Wallerian degeneration or myelin ovoids, we concluded that there is no length-dependent MF loss in $Gars^{P278KY/+}$ mice in the age group we studied. In the presence of well-defined abnormal NMJ morphology[27,43] and the current findings described here, the disease process in this model can best be classified as a distal terminal axonopathy.

Similar quantitative studies carried out in $Gars^{\Delta ETAQ/+}$ mice revealed that MF density increase per unit area of peripheral nerves was less conspicuous compared to $Gars^{P278KY/+}$ mice.
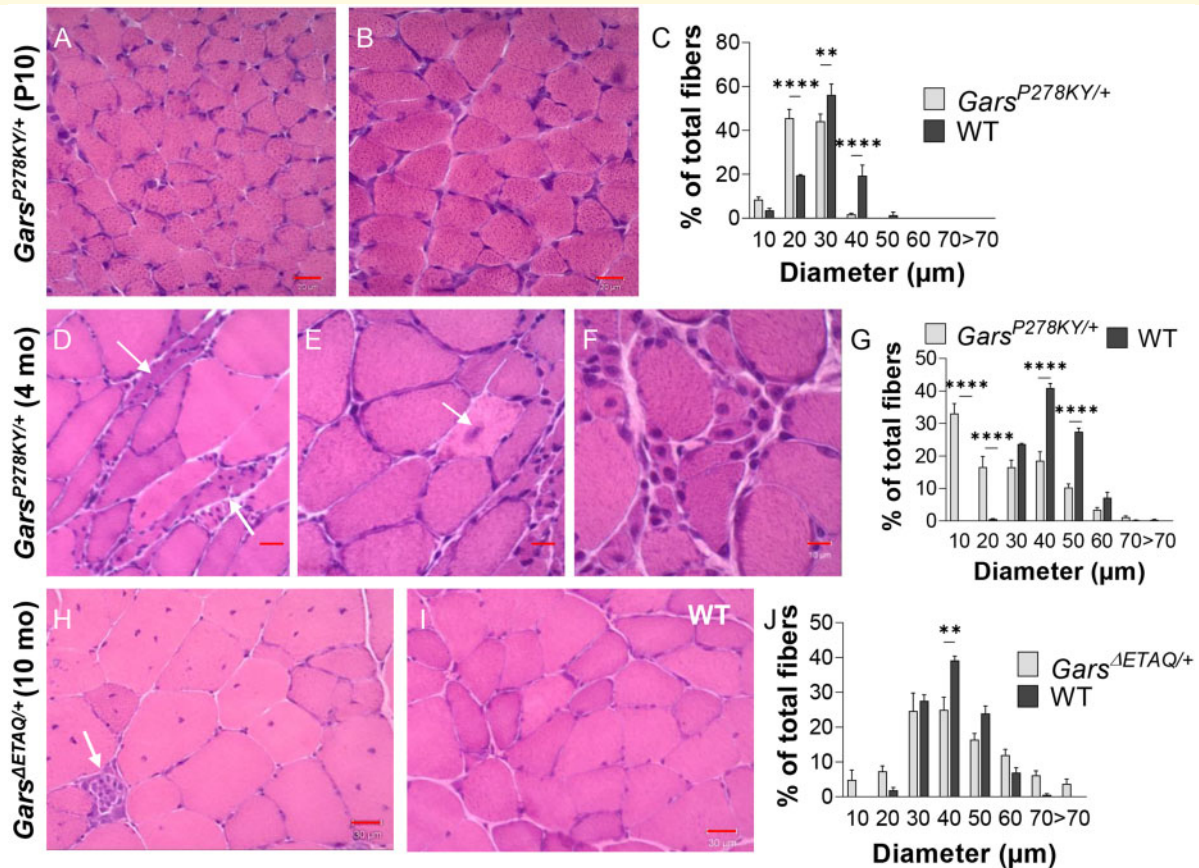
NT-3 improved myelin thickness in GARS mutants

Examination of 1 μm thick cross-sections from roots, sciatic and tibial nerves revealed an apparent increase in myelin thickness in the scAAV1.tMCK.NT-3-injected

$Gars^{P278KY/+}$ and $Gars^{\Delta ETAQ/+}$ mice compared to the untreated samples (Fig. 2A–D). At 12-week post-NT-3 gene transfer, g ratio (axon diameter/fibre diameter) of the MFs in the sciatic nerves from $Gars^{P278KY/+}$ mice showed an increase in myelin thickness corroborating the electrophysiological studies (Fig. 2E). The average g ratio in the Ringer's lactate-injected $Gars^{P278KY/+}$ mice ($Gars^{P278KY/+}$: 0.715 ± 0.002 versus WT: 0.61 ± 0.002, $P < 0.0001$) and $Gars^{\Delta ETAQ/+}$ mice ($Gars^{\Delta ETAQ/+}$: 0.691 ± 0.003 versus 0.624 ± 0.003, $P < 0.0001$) is significantly greater than that obtained from age-matched WT counterparts, reflecting the presence of thinner myelin in these models. In the AAV1.tMCK.NT-3-injected $Gars^{P278KY/+}$ mice, the g ratio was significantly reduced ($AAV1.NT-3$: 0.649 ± 0.002 versus untreated: 0.715 ± 0.002, $P < 0.0001$) and the percent of fibres with g ratio > 0.6 was down to 31%, which constituted about 59% of MFs in the untreated group (Fig. 2F). G ratio values obtained from $Gars^{\Delta ETAQ/+}$ mutant ($Gars^{\Delta ETAQ/+}$: 0.691 ± 0.003 versus $Gars^{P278KY/+}$: 0.715 ± 0.002; $P < 0.0001$) confirmed the microscopic observations that the extent of hypomyelination is more severe in the $Gars^{P278KY/+}$ mice. At 30 weeks post-AAV1.tMCK.NT-3 vector injection in the $Gars^{\Delta ETAQ/+}$ mice, the myelin thickness showed an increase for the axon size (Fig. 2G) with significantly reduced g ratio ($AAV1.NT-3$: 0.638 ± 0.003 versus untreated: 0.691 ± 0.003, $P < 0.0001$) and the percent fibres with g ratio > 0.6 reduced down to 23.4%, which constituted 48% of the MF population in the untreated cohort (Fig. 2H).

MF axon-size distribution histograms from sciatic nerves of $Gars^{P278KY/+}$ and $Gars^{\Delta ETAQ/+}$ mice showed NT-3 gene therapy had no effect on MF-axon size or number per unit area compared to the untreated cohort (Supplementary Fig. 6A–C).

NT-3 improved presynaptic axon terminal integrity at NMJ in the $Gars^{P278KY/+}$ mice

The $Gars^{P278KY/+}$ mice were reported to have abnormal NMJ morphology with a paucity of vesicles and mitochondria within distal terminal bulbs, impaired neuromuscular transmission due to presynaptic defect.[27,43] Using immunohistochemistry-based parameters illustrated previously[27] (Fig. 3A–C), we analysed an average of 88.6 NMJs per mouse from NT-3-treated and untreated $Gars^{P278KY/+}$ mice (n = 6 for both cohorts). This analysis showed that scAAV1.tMCK.NT-3 delivery in $Gars^{P278KY/+}$ mice at endpoint, following 12 weeks of treatment produced a 32% increase in the innervated NMJs (AAV1.NT-3: 69.52% ± 7.95 versus untreated: 37.48% ± 6.24, P = 0.0016). A decrease in the denervated and partially denervated/innervated NMJs were also noted (Fig. 3D).

Figure 4 Neuromyopathy in Gars mutants. Representative H&E-stained images of gastrocnemius muscle from $Gars^{P278KY/+}$ mice, shown in **A**, at P10 showing overall uniformly small fibres with mild size variability and **B** shows WT mice at P10. Scale bar = 20 μm. **C** shows muscle fibre size distribution graph comparing $Gars^{P278KY/+}$ and WT mice at P10. **D–F** shows muscles from 4 months old $Gars^{P278KY/+}$ mice showed marked fibre size variability with atrophic angular fibres, shown in **D** (arrows), rare fibres undergoing necrosis, shown in **E** (arrow) and exceedingly small fibres with prominent central nuclei, shown in **F**. Scale bar = 10 μm. **G** shows muscle fibre size histograms of the gastrocnemius muscle from $Gars^{P278KY/+}$ (3699 fibres, derived from $n = 6$) and age-matched WT (1364 fibres, $n = 4$) indicating a significant increase in small fibre population in $Gars^{P278KY/+}$ mice. Ongoing muscle fibre necrosis (arrow) was also present in $Gars^{\Delta ETAQ/+}$ mutant, shown in **H**, along with numerous hypertrophied fibres displaying multiple internal nuclei compared to WT muscle, shown in **I**. Fibre size distribution histograms from $Gars^{\Delta ETAQ/+}$ muscle (1793 fibres, $n = 6$) and age-matched WT (1287 fibres, $n = 4$) revealed that subpopulation of fibres with diameters <10 μm was much smaller in the $Gars^{\Delta ETAQ/+}$ mutant compared to $Gars^{P278KY/+}$, shown in **J**. Data are represented as mean ± SEM; two-way ANOVA, Sidak's multiple comparisons test. **$P < 0.01$, ****$P < 0.0001$.

Efficacy of NT-3 gene transfer therapy in muscles of $Gars^{P278KY/+}$ and $Gars^{\Delta ETAQ/+}$ mice

NT-3 improved neuromyopathy in $Gars^{P278KY/+}$ and $Gars^{\Delta ETAQ/+}$ mice

Compared to WT, muscles from $Gars^{P278KY/+}$ mice at postnatal Day 10 revealed overall uniformly small fibres with mild size variability with no evidence of muscle fibre breakdown as shown previously (Fig. 4A–C). In older $Gars^{P278KY/+}$ muscles, however, there was marked fibre size variability (Fig. 4D–G), atrophic angular (denervated) fibres (Fig. 4D), rare fibres undergoing necrosis (Fig. 4E) and exceedingly small fibres with prominent central nuclei (Fig. 4F), compatible with necrosis/regeneration cycles. We propose that these small round fibres

with diameters around 5 μm displaying prominent central nuclei are reminiscent of myotubes and their occurrence in small clusters may suggest impaired fusion events during regeneration.[44] Ongoing muscle fibre necrosis was also present in $Gars^{\Delta ETAQ/+}$ mutant along with numerous hypertrophied fibres displaying multiple internal nuclei compared to WT (Fig. 4H and I). Fibre size distribution histograms from $Gars^{P278KY/+}$ muscle revealed that over 30% of fibres had diameters <10 μm, while in the milder $Gars^{\Delta ETAQ/+}$ phenotype, this subpopulation was much smaller (Fig. 4G and J).

With NT-3 treatment, we found notable improvements in muscle histopathology in both mutants with apparent decreases in fibre subpopulations composed of abnormally small or hypertrophied ones (Fig. 5A and B). In the gastrocnemius muscle from $Gars^{P278KY/+}$ mice, the
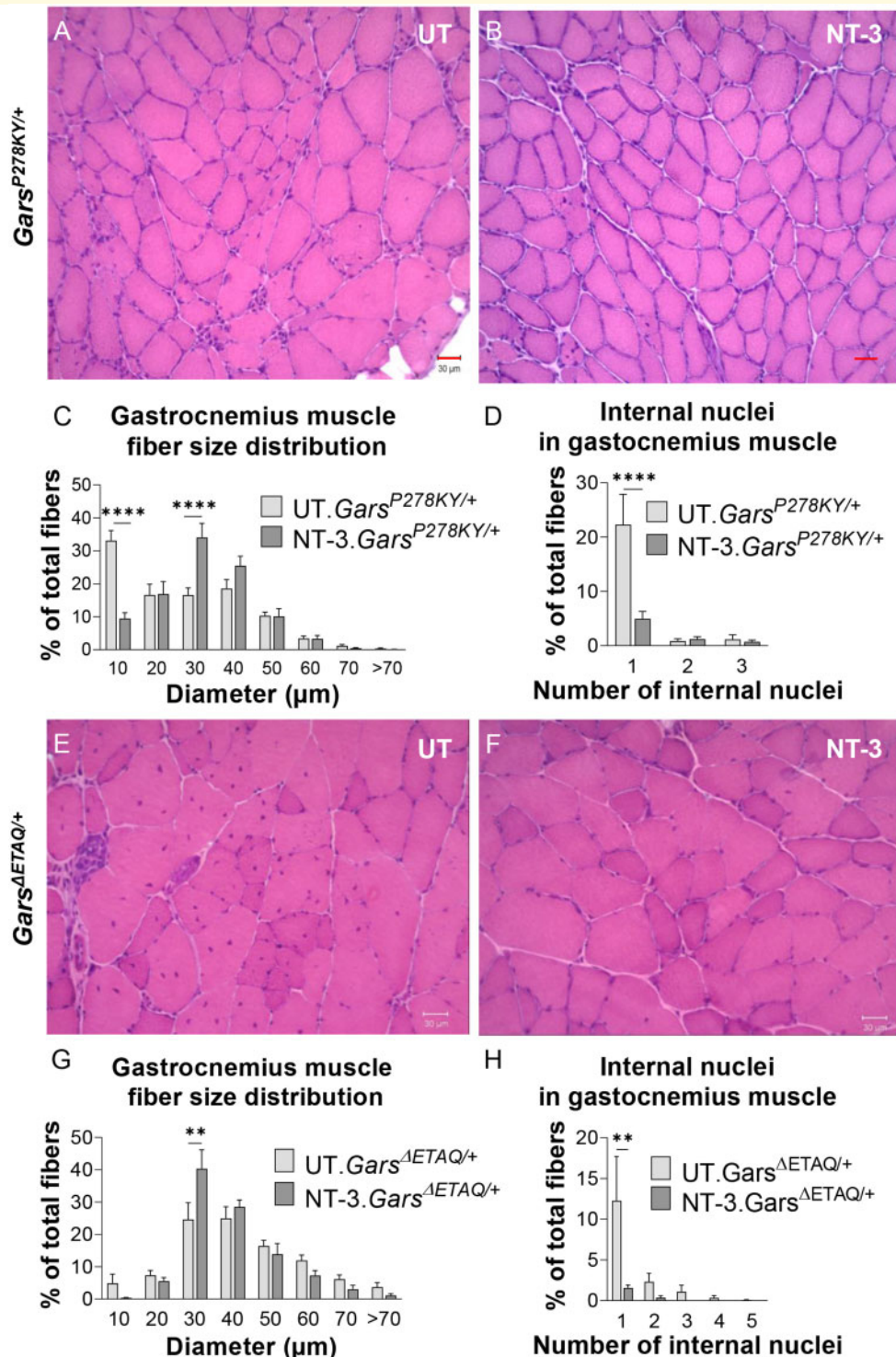
Figure 5 NT-3 gene transfer improves neuromyopathy in Gars mutants. Representative H&E images of gastrocnemius muscle from untreated, shown in **A**, and AAV1.NT-3-treated $Gars^{P278KY/+}$ mice, shown in **B**, showing a decrease in the number of abnormally small or hypertrophied fibres with treatment. Scale bar = 30 μm. **C** shows muscle fibre size distribution graph comparing the treated (3788 fibres, $n = 7$) and untreated (3699 fibres, $n = 6$) $Gars^{P278KY/+}$ mice showed a shift to larger diameter subgroups with NT-3 gene therapy. Bar graph showing a decrease in the number of internal nuclei in the gastrocnemius muscle from the treated ($n = 7$) compared to UT $Gars^{P278KY/+}$ mice ($n = 6$) is shown in **D**. Representative H&E images of gastrocnemius muscle from untreated, shown in **E**, and AAV1.NT-3-treated $Gars^{\Delta ETAQ/+}$ mice, shown in **F**, showing histopathological improvements with treatment. **G** shows muscle fibre size distribution graph comparing the treated (1443 fibres, $n = 4$) and untreated (1793 fibres, $n = 6$) $Gars^{\Delta ETAQ/+}$ mice showed an increase of fibres with mean fibre diameter in 30–40 μm range with NT-3 gene therapy. Bar graph showing a decrease in the number of internal nuclei in the gastrocnemius muscle from the treated ($n = 4$) compared to UT $Gars^{\Delta ETAQ/+}$ mice ($n = 6$) is shown in **H**. Data are represented as mean ± SEM; two-way ANOVA, Sidak's multiple comparisons test. **$P < 0.01$, ****$P < 0.0001$.
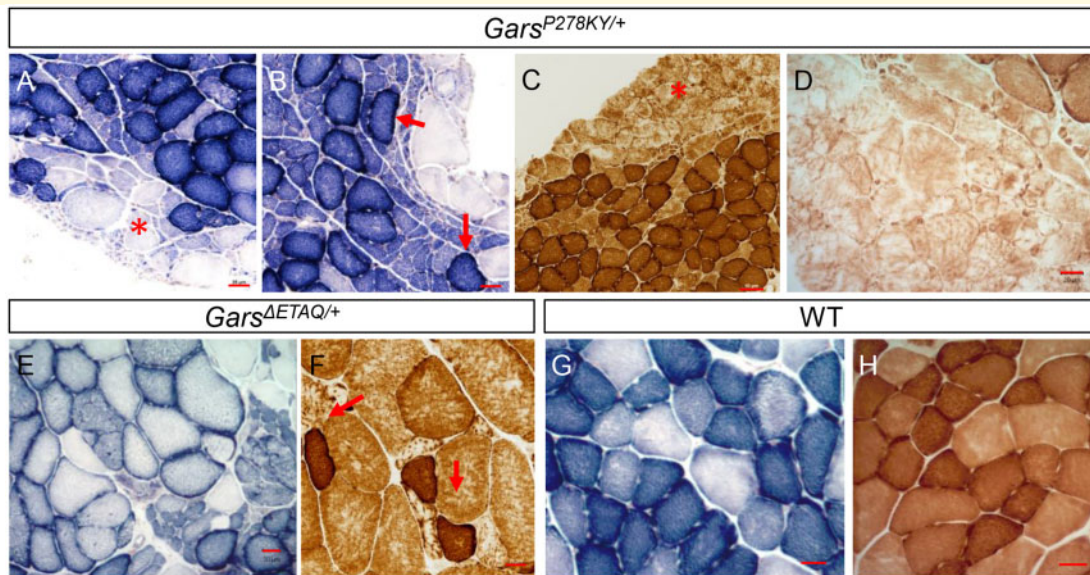
Figure 6 Abnormalities in muscle histochemistry using SDH and COX reactions in Gars mutants. **A**, **B** and **E** shows SDH and **C**, **D** and **F** shows COX staining in the gastrocnemius muscles from *Gars$^{P278KY/+}$*, shown in **A–D** and Gars$^{ΔETAQ/+}$ mutants showed reduced SDH and COX activities in fibres, most prominent at the superficial zones of the muscles of *Gars$^{P278KY/+}$* mice (asterisks) , shown in **E** and **F**. WT gastrocnemius SDH (**G**) and COX (**H**) activities are shown for comparison. Scale bar = 25 μm for **A**, **B**, **F**, **G** and **H**; 50 μm for **C**; 20 μm for **D**; 30 μm for **E**. Numerous ragged blue/brown fibres indicating increased mitochondria content in SDH and COX stains, respectively, were also noted (arrows).

smallest fibre population (with diameter <10 μm), constituting 33% of the total in the untreated cohort decreased down to 9.4% with NT-3 gene therapy (Fig. 5C). In addition, the NT-3 gene transfer resulted in a significant decrease in muscle fibres with internal nuclei (Fig. 5D). Further analysis upon gender stratification revealed that the largest percentage of small fibres is in the untreated males (Supplementary Fig. 7A). We observed similar histopathological improvements in *Gars$^{ΔETAQ/+}$* mutant with treatment (Fig. 5E–H, Supplementary Fig. 7B). Collectively, these findings show that the muscle pathology developed later in life in these Gars mutants is compatible with an ongoing neuromyopathic process and that NT-3 gene therapy attenuates these histopathological findings significantly.

Decreased oxidative phosphorylation markers in mutant Gars muscle is reversed with NT-3 gene therapy

Muscle histochemistry using SDH and COX reactions in the untreated *Gars$^{P278KY/+}$* mice revealed severely reduced SDH and COX activities in fibres, most prominent at the superficial zones of the gastrocnemius muscle, which are predominantly composed of type 2 or fast-twitch glycolytic fibres. Interestingly, there were numerous fibres with generous subsarcolemmal mitochondria content giving rise to the appearance of ragged blue/brown in SDH and COX stains, respectively (Fig. 6A–D). Compared to *Gars$^{P278KY/+}$* muscle, these findings were less prominent in the *Gars$^{ΔETAQ/+}$* mutant. GAS muscle from 10-month-old *Gars$^{ΔETAQ/+}$* mice showed hypertrophied fibres with decreased SDH activity, fibres with focal areas of loss of COX activity or ragged brown fibres (Fig. 6E and F) compared to WT (Fig. 6G and H). We observed a reversal of these findings with AAV1.NT-3 gene therapy as illustrated with COX stain in the superficial and deep zones of gastrocnemius muscles from *Gars$^{P278KY/+}$* (Fig. 7A–C) and *Gars$^{ΔETAQ/+}$* (Supplementary Fig. 8A and B) mutants.

Abnormalities in muscle enzyme histochemistry in Gars mutants suggested that mitochondrial dysfunction may play a role in muscle phenotype. To explore this further, we studied the expression levels of Cox1 and Cox3, which are mtDNA-encoded subunits of COX of respiratory complex IV and Atp5d. Real-time qPCR in untreated *Gars$^{P278KY/+}$* muscle (female and male combined) showed that Cox1 and Cox3 transcripts were approximately half and one-third the levels of age-matched WT controls, respectively (Fig. 7D and E). Atp5d transcripts were also significantly low, down to one-sixth of the WT (Fig. 7F). We found no sex difference for these transcripts in the *Gars$^{P278KY/+}$* mutant (Fig. 7D–F). In WT, however, Cox1 transcripts were found higher in females while males had 4.3-fold higher Atp5d transcripts than females (Fig 7F). Interestingly, compared to WT females, Atp5d expression in female *Gars$^{P278KY/+}$* muscle did not
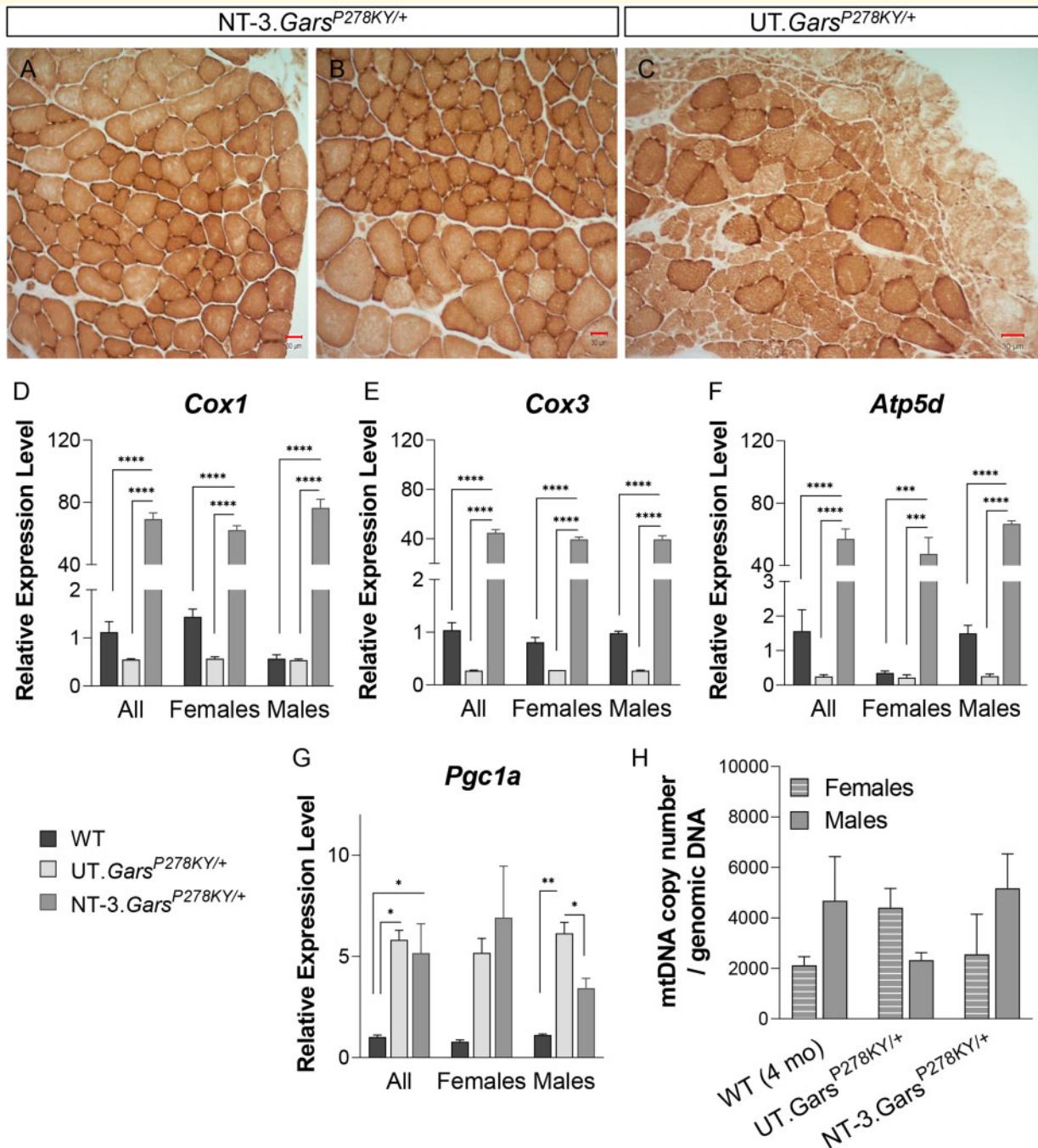
Figure 7 Muscle histochemistry in the NT-3-treated $Gars^{P278KY/+}$ mice and expression levels of mitochondrial proteins.
Representative images of COX-reacted sections from superficial, shown in **A**, and deep zones, shown in **B**, of gastrocnemius muscle in the treated $Gars^{P278KY/+}$ and untreated $Gars^{P278KY/+}$ mice, shown in **C**. WT control is depicted in Fig. 6H. Scale bar $= 30$ μm. NT-3 gene transfer therapy improved intensity and distribution of COX activity towards normalization. Bar graphs represent relative expression levels of *Cox1*, *Cox3*, *Atp5d* and *Pgc1a* and mtDNA copy number/genomic DNA in the treated and untreated $Gars^{P278KY/+}$ mice and age-matched WT mice showing both combined and gender-based data, shown in **D–H**. Data are represented as mean $\pm$ SEM; two-way ANOVA, Tukey's multiple comparisons test. $*P < 0.05$, $**P < 0.01$, $****P < 0.0001$; $n = 8$, NT-3.$Gars^{P278KY/+}$ mice; $n = 6$, UT.$Gars^{P278KY/+}$ mice; $n = 5$, WT (4 months).

change; in contrast, males showed significantly low expression, one-fifth of that in WT males. Most notably, the reversal of reduced COX staining in $Gars^{P278KY/+}$ muscle (Fig. 7A and B) was dramatically reflected in *Cox1*, *Cox3* and *Atp5d* expression levels following NT-3 gene

transfer showing over 70-, 40- and 50-fold increases in these transcripts, respectively, without sex difference (Fig. 7D–F).

We next assessed mitochondria biogenesis marker *Pgc1a* transcripts in relationship to mtDNA content in

gastrocnemius muscle from these Gars mutants. *Pgc1a* relative expression levels in $Gars^{P278KY/+}$ muscles were 5.7-fold higher than age-matched WT muscle with no sex difference (Fig. 7G). When both sexes were combined, we found no difference in mtDNA copy number per genomic DNA in muscles compared to age-matched WT counterparts. However, females showed higher mitochondria content than males, while in the WT, an opposite pattern was present, suggesting that male $Gars^{P278KY/+}$ muscle was not responding to increased *Pgc1a* expression in the same manner as female mice, correlating with much severe muscle involvement observed in male mice (Fig. 7H). *Pgc1a* relative expression levels in $Gars^{P278KY/+}$ muscles did not change in response to treatment although females showed higher transcripts than untreated counterparts (Fig. 7G). Interestingly, the mitochondria copy number appeared normalized with treatment showing a pattern observed in WT, males having higher mitochondria content than females (Fig. 7H).

Similar studies conducted in the untreated $Gars^{\Delta ETAQ/+}$ muscle at 10 months of age showed prominent decreases in relative expression levels of *Cox1*, *Cox3* and *Atp5d* without sex influence compared to age-matched WT muscle (Supplementary Fig. 9A–C). Interestingly, *Atp5d* transcripts from aged WT muscles did not show gender difference favouring males as seen in young WT muscle at 4 months of age although there was a trend for males having higher expression levels than females without reaching statistical difference (Fig. 6F, Supplementary Fig. 9C). *Pgc1a* expression was higher in the $Gars^{\Delta ETAQ/+}$ muscle compared to WT although this increase was modest, 1.6-fold and males showed higher levels than females without statistical significance (Supplementary Fig. 9D). No sex difference for mitochondria content in $Gars^{\Delta ETAQ/+}$ muscle or age-matched/old WT muscle was noted (Supplementary Fig. 9E). Collectively, these findings indicate that the primary myopathic process in these Gars mutants is associated with decreased oxidative phosphorylation markers compatible with mitochondria dysfunction. This finding is associated with increased *Pgc1a* expression, which we think is likely to be compensatory. NT-3 gene therapy increased oxidative phosphorylation markers dramatically along with reversing abnormalities in oxidative enzyme histochemistry in muscle. Moreover, we found that NT-3 gene therapy resulted in normalization, a reversal of mitochondria content of muscle towards WT patterns for both males and females.

Defective myoblast fusion in $Gars^{P278KY/+}$ mice

Our histopathological studies gave strong clues that myotubes expressing dominant GARS mutation display impaired fusion events and altered development of multinucleated myotubes. To explore this directly, myoblasts isolated from $Gars^{P278KY/+}$ mice muscles and WT controls were induced to differentiate to form *in vitro* myotubes. Three days after
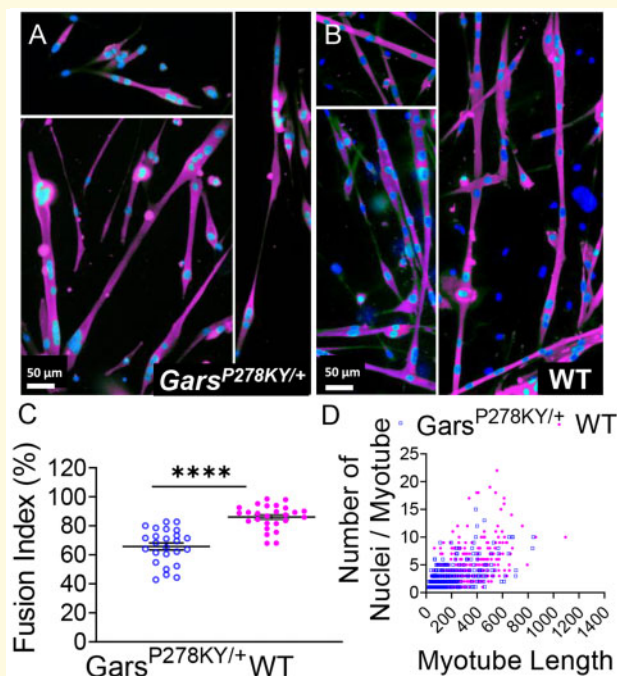

Figure 8 Myoblast fusion in $Gars^{P278KY/+}$ mice. Fluorescent images of myotubes differentiated from primary myoblast cultures isolated from 1-month-old, shown in **A**, $Gars^{P278KY/+}$ and WT mice, shown in **B**. Myotubes were stained with an anti-MHC antibody (red) and DAPI for nucleus (green), scale bar = 50 μm. Randomly selected areas were photographed at ×20 magnification. (Nikon Eclipse Ti2-E, Japan). A total of 710 myotubes from $Gars^{P278KY/+}$ mice and 659 myotubes from C57BL/6 mice were analysed (25–26 images derived from *n* = 2 mice in each group). Fusion index was significantly reduced in the $Gars^{P278KY/+}$ myoblasts (65.8%) compared to WT mice (86.1%), shown in **C**. Fusion index is a parameter used to assess the fusion capacity of myoblasts to form myotubes and calculated for each image as a percentage of the total number of nuclei in myotubes out of the total number of nuclei. Each data point represents fusion index calculated from randomly selected areas photographed at ×20 magnification. Error bars are ± SEM, $P < 0.0001$, unpaired *t*-test. Scattergram showing the myotube length and number of nuclei, shown in **D**. Overall, $Gars^{P278KY/+}$ myotubes were shorter and had fewer nuclei than WT.

the induction, the myotubes were stained with an anti-MHC antibody and a nuclear stain to count the number of nuclei that had been incorporated into multinucleated myotubes. Overall, a large fraction of $Gars^{P278KY/+}$ myotubes were shorter, ovoid shape with single nucleus or multiple clumped nuclei instead of the elongated shape seen in WT cells (Fig. 8A and B). We found a significant reduction of fusion competence between WT (86.1%) and $Gars^{P278KY/+}$ (65.8%) myoblasts ($P < 0.00001$; Fig. 8C). In addition, shorter $Gars^{P278KY/+}$ myotubes on average had more nuclei than WT myotubes; the opposite relationship was present for the longer WT myotubes having more nuclei than the mutant (Fig. 8D). Taken together, myoblast fusion assays demonstrate that both $Gars^{P278KY/+}$ mature myocytes and

myoblast progenitors are fusion defective. This defect likely contributes to the muscle phenotype in the $Gars^{P278KY/+}$ model.[38,45,46]

Discussion

Neuropathological features of $Gars^{P278KY/+}$ mutant were reported to include axonal loss, most of which occurs before 1 month of age; both motor and sensory axons are smaller. In addition, mutant mice have abnormal NMJ morphology with a paucity of vesicles and mitochondria within axon terminal bulbs, impaired neuromuscular transmission due to presynaptic defect and reduced nerve conduction velocity.[27,43] Recently, a comprehensive study in $Gars^{C201R/+}$ mutant showed that impaired NMJ maturation as an early defect preceded the loss of presynaptic terminals, leading to muscle denervation.[47] In this study, we introduced NT-3 gene transfer to $Gars^{P278KY/+}$ mice representing a severe phenotype at 4–6 weeks of age and to $Gars^{\Delta ETAQ/+}$ mice with a milder phenotype at 8–10 weeks of age and carried out a qualitative and quantitative assessment of NT-3 effect on the neuromuscular system 12 and 30 weeks post gene delivery, respectively. The treatment efficacy was less pronounced in the $Gars^{\Delta ETAQ/+}$ mutant despite a prolonged efficacy period; although it remains to be seen if the outcome measures can be improved with early onset treatment. We found no evidence of distal axon loss or degeneration in both mutants providing confirmatory evidence that the disease process is a distal-terminal axonopathy. This model of distal-terminal axonopathy is different from those previously reported, in which the disease process starts with membranous organelle accumulation and swelling of nerve terminals preceding degeneration and the process moves *pari-passu* proximally to distal nerves, internode by internode with nascent axon tip degeneration.[29,48–50] On the contrary, in the Gars mutants, the degenerative process appears to be confined to nerve terminals. The characteristic features of peripheral nerves, however, included reduced endoneurial cross-sectional area, reduced axon size with thin myelin and a remarkable increase in the number of MFs per unit endoneurial area, i.e. MF density. Moreover, comparative studies of peripheral nerves of Gars mutants at proximal and distal levels indicate that the actual number of MFs at these levels were not different from WT indicating that their numbers were not affected. We propose that there is a developmental delay in maturation of peripheral nerves, represented with radial growth stunt of axons as well as of other components of the endoneurium, therefore resulting in a density increase of MF population. We also recognized evidence of impaired/delayed maturation within axon–Schwann cell complexes of Remak bundles in the $Gars^{P278KY/+}$ mutant. At the ultrastructural level, immature polyaxonal aggregates engulfed by Schwann cell processes were common

suggesting that Schwann cells were halted at their immature state (Supplementary Fig. 10).

As we anticipated, NT-3 gene therapy did not affect MF density, nor did it significantly increase axon size. However, a reversal of hypomyelination was observed, increased myelin thickness was significant in both mutants, corresponding with the improvement in NCVs. The stimulating effect of NT-3 on mTOR pathways likely plays a major role in this process. The capacity of NT-3 targeting the translational machinery to stimulate myelin protein synthesis was first shown in oligodendrocyte primary cultures[51] and earlier studies have provided considerable evidence that mTORC1 has a role in regulating myelination in the CNS.[52–54] We observed similar effects of NT-3 on Schwann cells leading to improved myelin thickness in two other models of Charcot–Marie–Tooth subtypes previously,[20,28] and only in the Trembler J (Tr^J) model where there are secondary axonopathy and MF loss, NT-3 gene therapy improved regeneration and associated myelination process resulting in increased MF density.[20,55] It appears that overall NT-3 has corrective or normalizing effects on impaired biological processes until equilibrium or normalcy is established. In contrast, as we observed in toxicology studies for AAV1.NT-3 gene therapy and in studies by others, NT-3 does not affect nerve or muscle histology, nor does it alter functional recovery following crush injury in WT animals[56] suggesting that its effect is not directed to well-differentiated or normal functioning cells.[21,25] Specifically, extensive studies in AAV1.tMCK.NT-3-injected and untreated WT mice as part of Toxicology/Biodistribution studies and found no effects of NT-3 on MF size or density in sciatic nerves and no change in rotarod or grip strengths compared to untreated WT mice (part of this material was included to a review article[25]). In another publication in which we specifically described the effects of NT-3 gene therapy on the neurogenic muscle, we found no effect of NT-3 on the WT muscle size or fibre type composition.[21]

NT-3 is known to play a role in the functional maturation of neuromuscular synapses and is expressed in skeletal muscle as the predominant neurotrophin.[57–59] Studies in NT-3-deficient mice provided direct evidence that reduction in NT-3 availability during development impairs motor nerve terminal maturation and synaptic vesicle recycling and leads to a reduction in muscle fibre diameter.[60] In Gars mutants, the possibility of NT-3 deficiency state as in the amount and/or signalling through TrkC receptors in pertinent tissues seems plausible, requiring further investigation. Although an increase in the number of innervated NMJs in Gars$^{P278KY/+}$ mice with treatment was not entirely unexpected, the discovery of an ongoing myopathic process developed later in life in Gars mutants that was associated with mitochondria dysfunction was surprising. Reversal of muscle histopathology with robust increases in *Cox1*, *Cox3* and *Atp5d* expression levels following NT-3 gene transfer is foreseeable considering previously reported biological effects of NT-3 on Akt/mTORC1 and PGC1α

pathways. As we showed previously, AAV1.NT-3 gene therapy increased muscle fibre diameter through activation of the mTOR pathway and metabolic remodelling in the Tr^J model. In parallel, the expression levels of the mitochondrial biogenesis regulator Pgc1a, and the markers of glycolysis increased in the Tr^J muscle.[21] In this study, we found what appears to be a compensatory increase in Pgc1a relative expression levels in the untreated Gars$^{P278KY/+}$ muscles, which were over 5-fold higher than age-matched WT muscle with no sex difference. Mutant muscles from females showed higher mitochondria content than males, while an opposite pattern was present in the WT, suggesting that mutant muscle from males was not responding to increased Pgc1a expression in the same manner as females, correlating with the severe muscle involvement observed in males. We found no change in Pgc1a relative expression levels in Gars$^{P278KY/+}$ muscles in response to AAV.NT-3 gene therapy although interestingly, the mitochondria copy number appeared normalized, showing a pattern observed in WT, males having higher mitochondria content than females.

Compared to Gars$^{\Delta ETAQ/+}$ mutant with a milder phenotype, myopathic changes were more prominent in the Gars$^{P278KY/+}$ mice with striking fibre size variability, increased internal nuclei, rare fibres undergoing necrosis and very small fibres with prominent central nuclei reminiscent to myotubes. Muscle fibre size distribution histograms were bimodal, with males having a higher proportion of small fibres than females. Intriguingly, these myopathic changes in Gars mutants have a striking resemblance to the muscle pathology described in SMA mouse models resulting from SMN reduction in muscle including the early NMJ breakdown.[47,61–63] In one study, myopathy occurred as a late-onset, cell-autonomous consequence of low SMN in muscle, which was also associated with functional and structural defects in NMJs despite normal levels of SMN in other tissues.[61] These observations warrant further studies exploring whether SMN levels are affected by a globally repressed protein synthesis in the Gars$^{P278KY/+}$ mutant. In fact, the overall small size of Gars$^{P278KY/+}$ mice implies that besides peripheral nerves, other organ tissues including muscle are also subjected to stunted growth postnatally. Our own studies on semi-thick sections of spinal cord in Gars$^{P278KY/+}$ mice provide further support for this view, showing a visible increase in motor neuron density and smaller neuronal perikarya with scanty cytoplasm compared to WT (Supplementary Fig. 11).

Several pathogenic mechanisms have been proposed for GARS-linked Charcot–Marie–Tooth, in which the possibility that Charcot–Marie–Tooth-associated mutations in tRNA synthetases may all interfere with protein translation via a molecular mechanism independent of aminoacylation activity is supported by studies in Drosophila models.[16] In addition, with cytoplasmic and mitochondrial localization, mutant Gars inhibits translation in mitochondria in mice and patient-induced neuronal progenitor cells[17]. In favour of multifactorial pathogenic mechanisms, the concept that Gars mutants make aberrant interactions through the neomorphic surfaces leading to a toxic gain of function[64] has been supported by several studies. In one study, aberrant interactions of mutant Gars proteins with HDAC6 were shown, leading to hypo-acetylation of α-tubulin and axonal transport deficits.[65,66] Other studies described neomorphic interactions between mutant Gars with the cell-surface receptor Nrp1 on the motor neuron, interfering with the neurotrophic signalling of VEGF[67] or at the motor nerve terminal competing with Semaphorin-2a for binding to the cell-surface receptor plexin B.[68] It is interesting to note that P278KY GlyRS has been shown to interact with Nrp1[69] but that ΔETAQ GlyRS does not.[24] Aberrant interaction of mutant Gars with Trk receptors A/B/C in mice resulting destabilization of sensory neuron differentiation was also reported.[70] Further studies are needed to explore the exact roles of these neomorphic interactions between mutant Gars and their binding partners in relationship to the process of structural simplification and subsequent loss of axon terminals.

Nonetheless, we believe several main findings emerged from our studies. Of greatest interest, the late-onset myopathic process that we studied in these two Gars mutants is associated with mitochondria dysfunction, based on enzyme histochemistry and decreased markers of oxidative phosphorylation. Moreover, in primary myoblast cultures, we found that the consequence of Gars$^{P278KY/+}$ mutation is causing an intrinsic defect in muscle cell, manifesting with impairment of myoblast/myotube fusion. Collectively, these findings are suggestive of muscle cell-autonomous effects with mitochondria involvement in these two Gars models for autosomal dominant Charcot–Marie–Tooth disease type-2D. Our study identified the potential role of ATP-dependent pathways in the development of primary muscle pathology in Charcot–Marie–Tooth disease type-2D and from this perspective might provide additional support to a growing body of evidence suggesting mitochondria are likely to be a critical mediator of disease pathogenesis. Finally, our study shows that NT-3 gene transfer therapy in the Gars$^{P278KY/+}$ mice model of Charcot–Marie–Tooth disease type-2D leads to meaningful improvements in peripheral nerve myelination and NMJ integrity as well as in a unique myopathic process, associated with mitochondria dysfunction, all in combination contributing to functional outcome. Based on the multiple biological effects of this versatile molecule, we predict NT-3 has the potential to be beneficial in other ARS-linked Charcot–Marie–Tooth subtypes.

Supplementary material

Supplementary material is available at Brain Communications online.

Acknowledgements

Funding

Competing interests

The authors report no competing interests. Nationwide Children's Hospital has a financial relationship with Sarepta, the company who has optioned the technology related to the research described in this paper. ZS is the inventor of the technology discussed in this paper but has waived all future financial payments, including royalties, related to the technology. ZS is an inventor of another technology that is licensed to Sarepta by Nationwide Children's Hospital. The licensed technology is not related to the research described in this paper. In 2021, Nationwide Children's Hospital received a license payment from Sarepta for the unrelated technology and distributed a portion of the payment to ZS. ZS's relationship with Sarepta has been reviewed and approved by Nationwide Children's Hospital in accordance with its conflict of interest policies.

References

1. Antonellis A, Ellsworth RE, Sambuughin N, et al. Glycyl tRNA synthetase mutations in Charcot–Marie–Tooth disease type 2D and distal spinal muscular atrophy type V. *Am J Hum Genet.* 2003;72(5):1293–1299.
2. Del Bo R, Locatelli F, Corti S, et al. Coexistence of CMT-2D and distal SMA-V phenotypes in an Italian family with a GARS gene mutation. *Neurology.* 2006;66(5):752–754.
3. Dubourg O, Azzedine H, Verny C, et al. Autosomal-recessive forms of demyelinating Charcot–Marie–Tooth disease. *Neuromolecular Med.* 2006;8(1-2):75–86.
4. Sambuughin N, Sivakumar K, Selenge B, et al. Autosomal dominant distal spinal muscular atrophy type V (dSMA-V) and Charcot–Marie–Tooth disease type 2D (CMT2D) segregate within a single large kindred and map to a refined region on chromosome 7p15. *J Neurol Sci.* 1998;161(1):23–28.
5. Sivakumar K, Kyriakides T, Puls I, et al. Phenotypic spectrum of disorders associated with glycyl-tRNA synthetase mutations. *Brain.* 2005;128(Pt 10):2304–2314.
6. Wei N, Zhang Q, Yang XL. Neurodegenerative Charcot–Marie–Tooth disease as a case study to decipher novel functions of aminoacyl-tRNA synthetases. *J Biol Chem.* 2019;294(14):5321–5339.
7. Motley WW, Talbot K, Fischbeck KH. GARS axonopathy: Not every neuron's cup of tRNA. *Trends Neurosci.* 2010;33(2):59–66.
8. James PA, Cader MZ, Muntoni F, Childs AM, Crow YJ, Talbot K. Severe childhood SMA and axonal CMT due to anticodon binding domain mutations in the GARS gene. *Neurology.* 2006; 67(9):1710–1712.
9. Forrester N, Rattihalli R, Horvath R, et al. Clinical and genetic features in a series of eight unrelated patients with neuropathy due to glycyl-tRNA synthetase (GARS) variants. *J Neuromuscul Dis.* 2020;7(2):137–143.
10. Taylor RW, Pyle A, Griffin H, et al. Use of whole-exome sequencing to determine the genetic basis of multiple mitochondrial respiratory chain complex deficiencies. *JAMA.* 2014;312(1):68–77.
11. McMillan HJ, Schwartzentruber J, Smith A, et al. Compound heterozygous mutations in glycyl-tRNA synthetase are a proposed cause of systemic mitochondrial disease. *BMC Medical Genetics.* 2014;15:36.
12. Nafisinia M, Riley LG, Gold WA, et al. Compound heterozygous mutations in glycyl-tRNA synthetase (GARS) cause mitochondrial respiratory chain dysfunction. *PLoS One.* 2017;12(6):e0178125.
13. Oprescu SN, Chepa-Lotrea X, Takase R, et al. Compound heterozygosity for loss-of-function GARS variants results in a multisystem developmental syndrome that includes severe growth retardation. *Hum Mutat.* 2017;38(10):1412–1420.
14. Grice SJ, Sleigh JN, Motley WW, et al. Dominant, toxic gain-of-function mutations in gars lead to non-cell autonomous neuropathology. *Hum Mol Genet.* 2015;24(15):4397–4406.
15. Motley WW, Seburn KL, Nawaz MH, et al. Charcot–Marie–Tooth-linked mutant GARS is toxic to peripheral neurons independent of wild-type GARS levels. *PLoS Genet.* 2011;7(12):e1002399.
16. Niehues S, Bussmann J, Steffes G, et al. Impaired protein translation in *Drosophila* models for Charcot–Marie–Tooth neuropathy caused by mutant tRNA synthetases. *Nat Commun.* 2015;6:7520.
17. Boczonadi V, Meyer K, Gonczarowska-Jorge H, et al. Mutations in glycyl-tRNA synthetase impair mitochondrial metabolism in neurons. *Hum Mol Genet.* 2018;27(12):2187–2204.
18. Meier C, Parmantier E, Brennan A, Mirsky R, Jessen KR. Developing Schwann cells acquire the ability to survive without axons by establishing an autocrine circuit involving insulin-like growth factor, neurotrophin-3, and platelet-derived growth factor-BB. *J Neurosci.* 1999;19(10):3847–3859.
19. Sahenk Z, Nagaraja HN, McCracken BS, et al. NT-3 promotes nerve regeneration and sensory improvement in CMT1A mouse models and in patients. *Neurology.* 2005;65(5):681–689.
20. Sahenk Z, Galloway G, Clark KR, et al. AAV1.NT-3 gene therapy for Charcot–Marie–Tooth neuropathy. *Mol Ther.* 2014;22(3): 511–521.
21. Yalvac ME, Amornvit J, Chen L, Shontz KM, Lewis S, Sahenk Z. AAV1.NT-3 gene therapy increases muscle fiber diameter through activation of mTOR pathway and metabolic remodeling in a CMT mouse model. *Gene Ther.* 2018;25(2):129–138.
22. Wang B, Li J, Fu FH, et al. Construction and analysis of compact muscle-specific promoters for AAV vectors. *Gene Ther.* 2008; 15(22):1489–1499.
23. Mendell JR, Rodino-Klapac LR, Rosales XQ, et al. Sustained alpha-sarcoglycan gene expression after gene transfer in limb-girdle muscular dystrophy, type 2D. *Ann Neurol.* 2010;68(5):629–638.
24. Morelli KH, Griffin LB, Pyne NK, et al. Allele-specific RNA interference prevents neuropathy in Charcot–Marie–Tooth disease type 2D mouse models. *J Clin Invest.* 2019;129(12):5568–5583.
25. Sahenk Z, Ozes B. Gene therapy to promote regeneration in Charcot–Marie–Tooth disease. *Brain Res.* 2020;1727:146533.
26. Handschin C, Spiegelman BM. Peroxisome proliferator-activated receptor gamma coactivator 1 coactivators, energy homeostasis, and metabolism. *Endocr Rev.* 2006;27(7):728–735.
27. Seburn KL, Nangle LA, Cox GA, Schimmel P, Burgess RW. An active dominant mutation of glycyl-tRNA synthetase causes neuropathy in a Charcot–Marie–Tooth 2D mouse model. *Neuron.* 2006;51(6):715–726.
28. Ozes B, Myers M, Moss K, et al. AAV1.NT-3 gene therapy for X-linked Charcot–Marie–Tooth neuropathy type 1. *Gene Ther.* 2021. 10.1038/s41434-021-00231-3.
29. Sahenk Z, Mendell JR. Ultrastructural study of zinc pyridinethione-induced peripheral neuropathy. *J Neuropathol Exp Neurol.* 1979;38(5):532–550.
30. Sleigh JN, Grice SJ, Burgess RW, Talbot K, Cader MZ. Neuromuscular junction maturation defects precede impaired

lower motor neuron connectivity in Charcot–Marie–Tooth type 2D mice. *Hum Mol Genet*. 2014;23(10):2639–2650.

31. Lin W, Burgess RW, Dominguez B, Pfaff SL, Sanes JR, Lee KF. Distinct roles of nerve and muscle in postsynaptic differentiation of the neuromuscular synapse. *Nature*. 2001;410(6832):1057–1064.

32. Valdez G, Heyer MP, Feng G, Sanes JR. The role of muscle microRNAs in repairing the neuromuscular junction. *PLoS One*. 2014;9(3):e93140.

33. Wang L, Xu X, Jiang C, et al. mTORC1-PGC1 axis regulates mitochondrial remodeling during reprogramming. *FEBS J*. 2020; 287(1):108–121.

34. Chaignat E, Yahya-Graison EA, Henrichsen CN, et al. Copy number variation modifies expression time courses. *Genome Res*. 2011;21(1):106–113.

35. Jousse C, Muranishi Y, Parry L, et al. Perinatal protein malnutrition affects mitochondrial function in adult and results in a resistance to high fat diet-induced obesity. *PLoS One*. 2014;9(8):e104896.

36. Malik AN, Czajka A, Cunningham P. Accurate quantification of mouse mitochondrial DNA without co-amplification of nuclear mitochondrial insertion sequences. *Mitochondrion*. 2016;29:59–64.

37. Rooney JP, Ryde IT, Sanders LH, et al. PCR based determination of mitochondrial DNA copy number in multiple species. *Methods Mol Biol*. 2015;1241:23–38.

38. Yalvac ME, Amornvit J, Braganza C, et al. Impaired regeneration in calpain-3 null muscle is associated with perturbations in mTORC1 signaling and defective mitochondrial biogenesis. *Skelet Muscle*. 2017;7(1):27.

39. Hindi L, McMillan JD, Afroze D, Hindi SM, Kumar A. Isolation, culturing, and differentiation of primary myoblasts from skeletal muscle of adult mice. *Bio Protoc*. 2017;7:e2248.

40. Yalvac ME, Arnold WD, Hussain SR, et al. VIP-expressing dendritic cells protect against spontaneous autoimmune peripheral polyneuropathy. *Mol Ther*. 2014;22(7):1353–1363.

41. Spencer PS, Schaumburg HH. Ultrastructural studies of the dying-back process. IV. Differential vulnerability of PNS and CNS fibers in experimental central-peripheral distal axonopathies. *J Neuropathol Exp Neurol*. 1977;36(2):300–320.

42. Medori R, Autilio-Gambetti L, Monaco S, Gambetti P. Experimental diabetic neuropathy: Impairment of slow transport with changes in axon cross-sectional area. *Proc Natl Acad Sci USA*. 1985;82(22):7716–7720.

43. Spaulding EL, Sleigh JN, Morelli KH, Pinter MJ, Burgess RW, Seburn KL. Synaptic deficits at neuromuscular junctions in two mouse models of Charcot–Marie–Tooth type 2d. *J Neurosci*. 2016;36(11):3254–3267.

44. Karpati G, Molnar MJ. Muscle fibre regeneration in human skeletal muscle diseases. In Stefano Schiaffino, Terence Partridge eds. *Skeletal muscle repair and regeneration*. Dordrecht, Netherlands: Springer; 2008:199–216.

45. Chiu YH, Hornsey MA, Klinge L, et al. Attenuated muscle regeneration is a key factor in dysferlin-deficient muscular dystrophy. *Hum Mol Genet*. 2009;18(11):1976–1989.

46. Griffin DA, Johnson RW, Whitlock JM, et al. Defective membrane fusion and repair in Anoctamin5-deficient muscular dystrophy. *Hum Mol Genet*. 2016;25:1900–1911.

47. Sleigh JN, Mech AM, Schiavo G. Developmental demands contribute to early neuromuscular degeneration in CMT2D mice. *Cell Death Dis*. 2020;11(7):564.

48. Sahenk Z. Distal terminal axonopathy produced by 2,4-dithiobiuret: Effects of long-term intoxication in rats. *Acta Neuropathol*. 1990;81(2):141–147.

49. Sahenk Z, Mendell JR. Axoplasmic transport in zinc pyridinethione neuropathy: Evidence for an abnormality in distal turnaround. *Brain Res*. 1980;186(2):343–353.

50. Sahenk Z, Brown A. Weak-base amines inhibit the anterograde-to-retrograde conversion of axonally transported vesicles in nerve terminals. *J Neurocytol*. 1991;20(5):365–375.

51. Coelho RP, Yuelling LM, Fuss B, Sato-Bigbee C. Neurotrophin-3 targets the translational initiation machinery in oligodendrocytes. *Glia*. 2009;57(16):1754–1764.

52. Narayanan SP, Flores AI, Wang F, Macklin WB. Akt signals through the mammalian target of rapamycin pathway to regulate CNS myelination. *J Neurosci*. 2009;29(21):6860–6870.

53. Tyler WA, Gangoli N, Gokina P, et al. Activation of the mammalian target of rapamycin (mTOR) is essential for oligodendrocyte differentiation. *J Neurosci*. 2009;29(19):6367–6378.

54. Sherman DL, Krols M, Wu LM, et al. Arrest of myelination and reduced axon growth when Schwann cells lack mTOR. *J Neurosci*. 2012;32(5):1817–1825.

55. Sahenk Z, Yalvac ME, Amornvit J, et al. Efficacy of exogenous pyruvate in Trembler(J) mouse model of Charcot–Marie–Tooth neuropathy. *Brain Behav*. 2018;8(10):e01118.

56. Young C, Miller E, Nicklous DM, Hoffman JR. Nerve growth factor and neurotrophin-3 affect functional recovery following peripheral nerve injury differently. *Restor Neurol Neurosci*. 2001; 18(4):167–175.

57. Wang T, Xie K, Lu B. Neurotrophins promote maturation of developing neuromuscular synapses. *J Neurosci*. 1995;15(7 Pt 1): 4796–4805.

58. Lohof AM, Ip NY, Poo MM. Potentiation of developing neuromuscular synapses by the neurotrophins NT-3 and BDNF. *Nature*. 1993;363(6427):350–353.

59. Griesbeck O, Parsadanian AS, Sendtner M, Thoenen H. Expression of neurotrophins in skeletal muscle: Quantitative comparison and significance for motoneuron survival and maintenance of function. *J Neurosci Res*. 1995;42(1):21–33.

60. Sheard PW, Bewick GS, Woolley AG, et al. Investigation of neuromuscular abnormalities in neurotrophin-3-deficient mice. *Eur J Neurosci*. 2010;31(1):29–41.

61. Kim JK, Jha NN, Feng Z, et al. Muscle-specific SMN reduction reveals motor neuron-independent disease in spinal muscular atrophy models. *J Clin Invest*. 2020;130(3):1271–1287.

62. Cifuentes-Diaz C, Frugier T, Tiziano FD, et al. Deletion of murine SMN exon 7 directed to skeletal muscle leads to severe muscular dystrophy. *J Cell Biol*. 2001;152(5):1107–1114.

63. Dachs E, Hereu M, Piedrafita L, Casanovas A, Calderó J, Esquerda JE. Defective neuromuscular junction organization and postnatal myogenesis in mice with severe spinal muscular atrophy. *J Neuropathol Exp Neurol*. 2011;70(6):444–461.

64. He W, Zhang HM, Chong YE, Guo M, Marshall AG, Yang XL. Dispersed disease-causing neomorphic mutations on a single protein promote the same localized conformational opening. *Proc Natl Acad Sci USA*. 2011;108(30):12307–12312.

65. Mo Z, Zhao X, Liu H, et al. Aberrant GlyRS-HDAC6 interaction linked to axonal transport deficits in Charcot–Marie–Tooth neuropathy. *Nat Commun*. 2018;9(1):1007.

66. Benoy V, Van Helleputte L, Prior R, et al. HDAC6 is a therapeutic target in mutant GARS-induced Charcot–Marie–Tooth disease. *Brain*. 2018;141(3):673–687.

67. He W, Bai G, Zhou H, et al. CMT2D neuropathy is linked to the neomorphic binding activity of glycyl-tRNA synthetase. *Nature*. 2015;526(7575):710–714.

68. Grice SJ, Sleigh JN, Zameel Cader M. Plexin-semaphorin signaling modifies neuromuscular defects in a *Drosophila* model of peripheral neuropathy. *Front Mol Neurosci*. 2018;11:55.

69. Sleigh JN, Gómez-Martín A, Wei N, Bai G, Yang X-L, Schiavo G. Neuropilin 1 sequestration by neuropathogenic mutant glycyl-tRNA synthetase is permissive to vascular homeostasis. *Sci Rep*. 2017;7(1):9216.

70. Sleigh JN, Dawes JM, West SJ, et al. Trk receptor signaling and sensory neuron fate are perturbed in human neuropathy caused by *Gars* mutations. *Proc Natl Acad Sci USA*. 2017;114(16): E3324–E3333.